Research Article

Olga Friesen*, Leander Claes, Jonas Hölscher, Bernd Henning, Claus Scheidemann, Tobias Hemsel, Raphael Kuess, Andrea Walther, Carsten Spieker and Jens Förstner

# Measurement of multiphysical material parameters of piezoceramic components for high-power ultrasonic applications

Messtechnische Charakterisierung multiphysikalischer Materialparameter von piezokeramischen Bauteilen für Hochleistungs-Ultraschallanwendungen

https://doi.org/10.1515/teme-2026-0042
Received April 9, 2026; accepted May 13, 2026;
published online June 4, 2026

**Abstract:** Simulation-based design of high-power ultrasonic systems depends on the accurate modelling of the electromechanical behaviour of piezoceramic materials. In practical transducer applications, the relevant operating points are influenced by mechanical preload and heating, both of which give rise to changes in the elastic, dielectric, and piezoelectric material properties. Material parameters identified under idealised, unloaded conditions are therefore insufficient to represent piezoceramic material behaviour under realistic operating conditions. To overcome this limitation, experimental setups are developed that enable the measurement of electrical impedance spectra under controlled thermal and mechanical conditions. The acquired impedance data are used in an inverse identification procedure, in which the behaviour of a finite element forward model is iteratively fitted to the measurements using a block coordinate descent optimisation strategy guided by a sensitivity analysis. This yields effective linear material parameters as a function of temperature and mechanical stress at varying operating points. The identified temperature-dependent parameters, for instance, can be employed in a coupled thermo-electromechanical simulation framework to predict the temperature-dependent material behaviour during operation. The linear identification based on varying operation points provides an initial approximation of the nonlinear material response, establishing a basis for the development of corresponding nonlinear material models.

**Keywords:** piezoceramic materials; inverse identification; sensitivity analysis; temperature dependence; mechanical preload; nonlinear material behaviour

**Zusammenfassung:** Das simulationsgestützte Design von Hochleistungs-Ultraschallsystemen ist maßgeblich von der präzisen Modellierung des elektromechanischen Verhaltens piezokeramischer Materialien abhängig. In realen Wandleranwendungen werden die relevanten Arbeitspunkte des Materials durch mechanische Vorspannung und Erwärmung bestimmt, die Änderungen der elastischen, dielektrischen und piezoelektrischen Materialeigenschaften hervorrufen. Unter idealisierten, lastfreien Bedingungen identifizierte Materialparameter sind daher nicht ausreichend, um das Verhalten von Piezokeramiken unter realistischen Betriebsbedingungen abzubilden. Um dieser Einschränkung zu begegnen, werden experimentelle Aufbauten entwickelt, die die Messung elektrischer Impedanzspektren unter kontrollierten thermischen und mechanischen Bedingungen ermöglichen. Die erfassten Impedanzdaten dienen als Eingangsgrößen für ein inverses Identifikationsverfahren, bei dem das Verhalten eines Finite-Elemente-Modells mithilfe von Optimierungsstrategien im Blockkoordinaten-Abstiegsverfahren iterativ an die Messungen angepasst wird. Grundlage hierfür ist eine systematische Sensitivitätsanalyse der Modellparameter. Das Verfahren liefert effektive, lineare Materialparameter in Abhängigkeit von Temperatur und mechanischer

***Corresponding author: Olga Friesen**, Measurement Engineering Group, Paderborn University, Paderborn, Germany,
E-mail: friesen@emt.uni-paderborn.de.
https://orcid.org/0009-0007-5598-9484
**Leander Claes, Jonas Hölscher and Bernd Henning**, Measurement Engineering Group, Paderborn University, Paderborn, Germany
**Claus Scheidemann and Tobias Hemsel**, Chair of Dynamics and Mechatronics, Paderborn University, Paderborn, Germany
**Raphael Kuess and Andrea Walther**, Mathematical Optimization, Humboldt-Universität zu Berlin, Berlin, Germany
**Carsten Spieker and Jens Förstner**, Theoretical Electrical Engineering Group, Paderborn University, Paderborn, Germany

Vorspannung in unterschiedlichen Arbeitspunkten. Die identifizierten temperaturabhängigen Parameter können in einer gekoppelten thermo-elektromechanischen Simulation eingesetzt werden, um das Materialverhalten während des Betriebs vorherzusagen. Die auf Arbeitspunkte basierende lineare Identifikation ermöglicht eine erste Approximation des nichtlinearen Materialverhaltens und bildet die Grundlage für die Entwicklung entsprechender nichtlinearer Materialmodelle.

**Schlagwörter:** Piezokeramische Materialien; Inverse Identifikation; Sensitivitätsanalyse; Temperaturabhängigkeit; mechanische Vorspannung; nichtlineares Materialverhalten

# 1 Introduction

The results reported in this article represent a cross-section of the first phase of the DFG Research Unit FOR 5208 NEPTUN (Model-based determination of the nonlinear properties of piezoceramics in high-power ultrasonic applications). The research unit is dedicated to the systematic characterisation and nonlinear modelling of piezoceramic materials using inverse measurement procedures, and comprises an interdisciplinary group of researchers from the fields of pure and applied mathematics, as well as mechanical and electrical engineering.

High-power ultrasonic systems are widely used in industrial manufacturing, joining processes, and medical devices. The performance of such systems depends on the resonant electromechanical behaviour of transducers based on piezoelectric elements. In current development processes, numerical simulations are employed to predict resonance frequencies and mode shapes, thereby contributing to cost reduction and a decrease in the number of iterative prototype design phases [1]–[3]. However, the accuracy of such simulations is fundamentally dependent on the quality and consistency of the underlying material models and a precise knowledge of the material properties of the sample in question.

Piezoelectric ceramics, which form the basis of such ultrasonic transducers, operate under strongly coupled electromechanical conditions and are often subjected to static mechanical stresses and heating during operation. These influencing factors shift the effective operating point of the sample, altering its elastic, dielectric, and piezoelectric properties and significantly increase the complexity of the material model [4], [5]. Consequently, material parameters determined under idealised experimental conditions may not accurately reflect the behaviour within a real transducer device. The challenge therefore lies not only in formulating multiphysical models that capture the interaction of the underlying physical effects, but also in determining consistent material parameters under realistic operating conditions.

Since the relevant material properties cannot be measured directly under operational conditions, an inverse identification strategy is adopted, in which system responses such as the electrical impedance spectrum are measured experimentally and used to determine parameters at different operating points. In this approach, impedance measurements are compared with a numerical finite element model, enabling the identification of effective material parameters under varying mechanical and thermal conditions. The resulting linear parameter sets can subsequently be used to investigate nonlinear behaviour through initial experimental and numerical studies, providing insights into the emerging nonlinear effects and facilitating the development of suitable material models.

Beyond the well-established piezoceramic materials such as PZT (lead zirconate titanate), there is an increasing focus on lead-free alternatives. The requirement for sustainable substitute materials is driven by European environmental and chemicals regulations, such as RoHS and REACH. In the context of high-power ultrasonic transducer applications, only a limited number of potentially viable lead-free materials are currently available, among them ceramics based on KNN (potassium sodium niobate) such as PIC753 and PIC758 (PI Ceramic, Germany). Due to their comparatively recent market introduction, their linear material properties have not yet been fully characterised [6]. With regard to nonlinear behaviour, preliminary studies suggest that the effects are less pronounced in lead-free materials compared to PZT [7], though a systematic characterisation under typical operating conditions remains to be conducted. The methods developed in this work are therefore designed with applicability to both established and emerging piezoceramic materials in mind.

This article presents a selection of results from the first phase of the DFG Research Unit FOR 5208 NEPTUN, in which the inverse measurement procedure plays a fundamental role in the model-based characterisation of piezoceramic materials. The objective of this study is to illustrate how experimental impedance-based measurement procedures, in conjunction with sensitivity-based optimisation strategies, enable the identification of consistent and complete sets of material parameters for piezoceramic materials under application-relevant operating conditions. The inverse identification approach introduced here represents a significant methodological advance, as it enables the characterisation of piezoceramic materials under realistic operating conditions using a single sample. The structure of the article is as follows: Section 2 introduces the mathematical material models underlying the identification approach. Section 3 describes the experimental setups developed for temperature- and stress-dependent impedance measurements. The inverse parameter identification procedure is detailed in Section 4, followed by the presentation and discussion of results in Section 5. Section 6 addresses first steps towards nonlinear material modelling, and Section 7 provides concluding remarks.

# 2 Mathematical models

The mathematical framework underlying the identification approach developed in this work is established in this section. The linear piezoelectric material model introduced in Subsection 2.1 forms the basis of the finite element forward model employed in the inverse procedure. Building on this, the second subsection describes the thermal effects arising from mechanical losses, which couple the electromechanical and thermal fields and motivate the temperature-dependent parameter identification.

## 2.1 Linear models for piezoelectric material

In this study, the behaviour of piezoceramic materials is described in terms of linear piezoelectricity. Adopting Voigt's notation [8], mechanical and electrical field quantities are coupled by linear constitutive Equations (1a) and (1b)

$$\boldsymbol{T} = -\underline{\boldsymbol{e}}^{\mathsf{T}}\boldsymbol{E} + \underline{\boldsymbol{c}}^{E}\boldsymbol{S} + \alpha_K\underline{\boldsymbol{c}}^{E}\partial_t\boldsymbol{S} \tag{1a}$$

$$\boldsymbol{D} = \underline{\boldsymbol{\varepsilon}}^{S}\boldsymbol{E} + \underline{\boldsymbol{e}}\boldsymbol{S}, \tag{1b}$$

where $\boldsymbol{T}$ and $\boldsymbol{S}$ denote mechanical stress and strain, respectively, and $\boldsymbol{E}$ and $\boldsymbol{D}$ represent the electrical field strength and displacement. Losses are accounted for by a scalar Kelvin-Voigt model [9], [10], which is found to be sufficient for the modelling of low-damping piezoelectric materials [11]. The material behaviour is characterised by a set of material parameters: the elasticity $\underline{\boldsymbol{c}}^{E}$, dielectric $\underline{\boldsymbol{\varepsilon}}^{S}$ and piezoelectric coefficient $\underline{\boldsymbol{e}}$ matrices, as well as the parameter $\alpha_K$ quantifying Kelvin-Voigt damping. The superscripts $E$ and $S$ denote a description assuming constant electric field and constant mechanical strain conditions, respectively, and the superscript T denotes transposition. Applying the symmetry conditions of a transversely isotropic material, 11 independent material parameters are to be determined:

$$\begin{aligned}\boldsymbol{p}_{\mathrm{mat}} = \big[&c_{11}^{E}, c_{12}^{E}, c_{13}^{E}, c_{33}^{E}, c_{44}^{E},\\ &\varepsilon_{11}^{S}, \varepsilon_{33}^{S}, e_{15}, e_{31}, e_{33}, \alpha_K\big].\end{aligned} \tag{2}$$

In the current study, the density $\rho$ is obtained directly from measurements and is therefore not included in the parameter vector. The density is assumed constant across the investigated temperature and stress ranges, as the resulting variations are considered negligible compared to those of the other material parameters.

Finite element numerical simulations of this linear model are well established [12] and form the basis of the forward model employed in the inverse identification procedure described in Section 4. In addition the utilisation of the discontinuous Galerkin time-domain method (DG) has been analysed in a previous study [13]. This method can be advantageous when simulating complex three-dimensional structures but for the present work the classical finite element method is used. For the assumed material model including Kelvin-Voigt damping, the time-dependent elastic behaviour is described by the viscous wave equation, in which losses arise from a mixed third-order derivative term. The electrical behaviour is described by the electrostatic equations. It is important to note, however, that the constitutive equations (1) represent a linearisation at a specific thermodynamic state. In actual high-power operation, piezoceramic components are subjected to static mechanical stress and heating during operation. Consequently, the effective material coefficients may be dependent on the respective operating conditions.

## 2.2 Thermal effects of mechanical losses

The mechanical losses introduced in Subsection 2.1 result in a conversion of kinetic to thermal energy, which in turn affects the material behaviour through temperature-dependent material properties. Based on the first law of thermodynamics, this energy conversion can be quantified via the power density $P$ in the solid, given by the inner product of the stress field and the temporal derivative of the strain field [14]:

$$P = \boldsymbol{T}^{\mathsf{T}}\partial_t\boldsymbol{S}. \tag{3}$$

Inserting Equation (1a) yields the expression

$$P = -\boldsymbol{E}^{\mathsf{T}}\underline{\boldsymbol{e}}\partial_t\boldsymbol{S} + \boldsymbol{S}^{\mathsf{T}}\big(\underline{\boldsymbol{c}}^{E}\big)^{\mathsf{T}}\partial_t\boldsymbol{S} + \alpha_K\partial_t\boldsymbol{S}^{\mathsf{T}}\big(\underline{\boldsymbol{c}}^{E}\big)^{\mathsf{T}}\partial_t\boldsymbol{S}. \tag{4}$$

The first and second term describe lossless, bidirectional electromechanical power conversion and storage, respectively [15]. For oscillatory strain fields, especially the second term ($\boldsymbol{S}^{\mathsf{T}}(\underline{\boldsymbol{c}}^{E})^{\mathsf{T}}\partial_t\boldsymbol{S}$) can be shown to have no static component. Only the third term yields a non-zero temporal average and thus contributes to heat generation. This term can be inserted directly into the differential equation for the temperature field $\vartheta$:

$$\rho c_p\partial_t\vartheta - \lambda_{\mathrm{th}}\Delta\vartheta = \alpha_K\partial_t\boldsymbol{S}^{\mathsf{T}}\big(\underline{\boldsymbol{c}}^{E}\big)^{\mathsf{T}}\partial_t\boldsymbol{S}, \tag{5}$$

with the specific heat capacity $c_p$ and the thermal conductivity $\lambda_{\mathrm{th}}$. In long-term time-domain simulations, solutions to Equation (5) can be used to account for local changes in material properties, provided that a temperature-dependent formulation for the parameters $\boldsymbol{p}_{\mathrm{mat}}(\vartheta)$ can be identified. The results of this approach are shown in Subsection 5.2.

## 3 Experimental setups

The material model introduced in Section 2 requires the identification of effective material parameters under realistic operating conditions. Two experimental setups are thus developed, each targeting one of the primary influencing factors. The specimens under investigation are hard piezoceramic rings of two material types – PIC181 and PIC184 (PI Ceramic, Germany) – in two different geometries. The dimensions of each specimen are specified alongside the respective results. In addition to the thermal and mechanical investigations presented here, experiments under electrical preload are conducted [16]. A temperature-controlled measurement setup, enabling the acquisition of impedance spectra across a defined temperature range, is described in Subsection 3.1. Subsection 3.2 includes a mechanically preloaded transducer configuration designed to characterise the stress-dependent material behaviour. In both cases, the measured impedance spectra subsequently serve as input to the inverse parameter identification.

### 3.1 Temperature-dependent impedance measurements

To analyse the material behaviour of piezoceramic samples under controlled thermal conditions, a test setup was developed [17], shown schematically in Figure 1. The sample is placed in a temperature-controlled chamber, which ensures a stable and reproducible thermal environment throughout the measurement process. The temperature is controlled by a thermostat system (Magio MS-310F, Julabo, Germany). A temperature sensor is positioned close to the sample, thus enabling the monitoring of the temperature in the vicinity of the sample without a physical contact, thereby ensuring that the vibrations of the specimen are not disturbed during the measurements. To ensure a homogeneous temperature distribution within the chamber, active ventilation is used to achieve uniform heating of the samples. The impedance measurements are performed over a temperature range of 25 °C to 85 °C in increments of 5 K using an impedance analyser (E4990A, Keysight Technologies, USA).

The thermostat and the impedance analyser are remotely controlled, enabling automated measurement

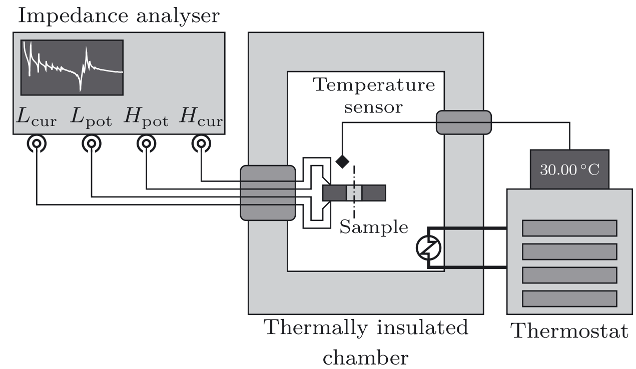


**Figure 1:** Experimental setup for temperature-dependent impedance measurements.

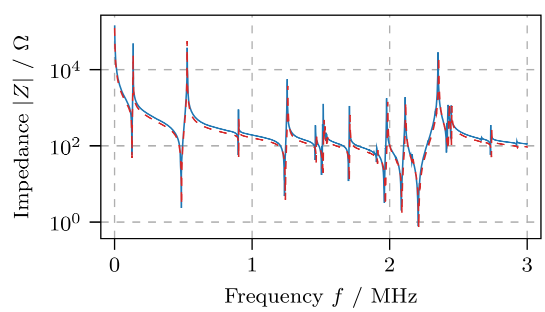


**Figure 2:** Measurements of impedance spectra of a PIC181 piezoceramic ring with a thickness $t$ of 1 mm, an outer radius $r_{\mathrm{o}}$ of 6.35 mm, and an inner radius $r_{\mathrm{i}}$ of 2.6 mm for 25 °C ——— and 85 °C – – – .

sequences across the entire temperature range. Each measurement is performed after a sufficient time for thermal equilibration, ensuring that a homogeneous temperature distribution within the chamber can be assumed.

Figure 2 exemplarily shows the impedance response measured at 25 °C and 85 °C. The characteristic resonances are clearly visible, manifesting as local minima (resonance frequencies) followed by local maxima (antiresonance frequencies). Each resonance pertains to eigenmodes of the sample in a specific spatial direction [18]. Temperature variations lead to slight shifts in these frequencies, particularly in the frequency range above 1 MHz. The influence of temperature appears relatively small, which is partly attributable to the resolution of the graphical representation. Nevertheless, even these moderate shifts correspond to variations in the effective material parameters, which are discussed in Subsection 5.1.

### 3.2 Impedance measurements under mechanical stress

A transducer-based test setup is developed to investigate the influence of mechanical stress on the effective material behaviour of piezoceramic samples. Preliminary

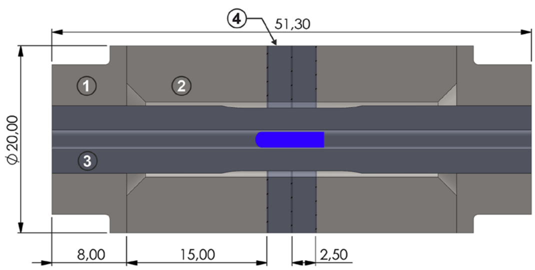


**Figure 3:** Cross-sectional view of the measurement transducer consisting of nuts (1), end masses (2), hollow steel bolt (3), piezoceramic rings (4), and strain gauge (highlighted in blue). All lengths are given in millimetres. The cables of the strain gauge are omitted for clarity.

investigations using hydrostatic pressure generated by supercritical argon are conducted [17]. However, the experimentally realisable hydrostatic loading is limited to approximately 15 MPa, which neither represents the uniaxial preload conditions typically present in ultrasonic transducers nor reaches the stress levels from 40 MPa to 80 MPa common in such devices. For this reason, a classical mechanically preloaded transducer configuration is selected, which allows a defined axial stress to be applied directly to the piezoceramic rings.

The setup shown in Figure 3 is based on a symmetric transducer design (known as Langevin-type transducer) consisting of two end masses, two nuts, and two ring-shaped piezoceramic samples and a hollow steel bolt. The piezoceramic rings are clamped between the metallic end masses by means of a screw connection. The hollow bolt has an outer diameter of 6.7 mm at the centre of the transducer and the inner diameter of the piezoelectric rings is 8 mm, resulting in an air-gap with a width of 0.65 mm. The geometric dimensions of the end masses are determined by a study based on finite element simulations so that a nearly homogeneous normal stress distribution is achieved within the piezoceramic rings. Measured geometrical deviations of the fabricated components from the nominal dimensions do not exceed 0.05 mm, corresponding to relative deviations of less than 0.5 %. Measurements of the resulting preload distribution using pressure-sensitive films (FUJIFILM, pressure measurement film, type HS, Japan) are used to confirm the numerical results. There are no pronounced local stress concentrations; the deviation of the preload distribution across the surface of the ceramics is below 1 %.

To monitor the applied stress, a strain gauge (HBM TB21, Germany) is bonded inside the hollow steel bolt using an adhesive. The strain gauge signal is recorded using an amplifier (HBM MGCplus, Germany), which allows the applied preload to be monitored during assembly and measurement. The preload levels (40 MPa, 50 MPa, and 60 MPa) are set mechanically and measured via the strain gauge signal. After assembling the transducer and applying the desired preload, the electrical impedance response, the ambient temperature, and the remaining preload have been measured over time to capture the time-dependent changes in the impedance characteristics. The impedance responses are measured automatically every 30 min under small-signal excitation (25 mV) and free-vibration condition using an impedance analyser (HP4192A, Keysight Technologies, USA), while the ambient temperature is measured every 5 min throughout the entire measurement period, with temperature fluctuations not exceeding ($\pm$1 K). This procedure enables a consistent evaluation of the time-dependent stabilisation behaviour after assembly and preload application. The characteristic quantities of the impedance response, in particular the resonance frequency, the antiresonance frequency, and the impedance magnitude are evaluated. The results shown exemplarily for a PIC184 (PI Ceramic, Germany) ring-shaped piezoceramic sample with an outer diameter of 20 mm in Figures 4 and 5 reveal a clear dependence of the measured response on the applied mechanical preload. With increasing preload, both the resonance and antiresonance frequencies shift systematically towards higher values, indicating an increase in the stiffness of the piezoceramic elements. The electromechanical coupling factor can be derived from the frequency difference between resonance and antiresonance. In the present measurements, this difference decreases over time, resulting in a measurable reduction of the coupling factor. For instance, at a preload of 40 MPa, the effective coupling factor decreases by approximately 6 % within 50 h. At the same time, the impedance magnitude decreases, particularly in the vicinity of the resonance minimum. In addition to the preload dependence, a pronounced time-dependent behaviour is observed after preload application. For preload levels of 40 MPa and 50 MPa, the resonance and antiresonance frequencies exhibit a gradual increase over time, which follows an approximately linear trend on a logarithmic time scale. In contrast, for a preload level of 60 MPa, a superlinear trend is observed, indicating a deviation from the behaviour at lower preload levels. Overall, the results demonstrate that both the magnitude of the applied preload and the elapsed time after assembly significantly influence the measured impedance characteristics. This highlights the necessity of considering time-dependent stabilisation effects when performing reliable parameter identification of piezoelectric materials under mechanical stress [19]. Investigating the causes of these effects is subject of future research.

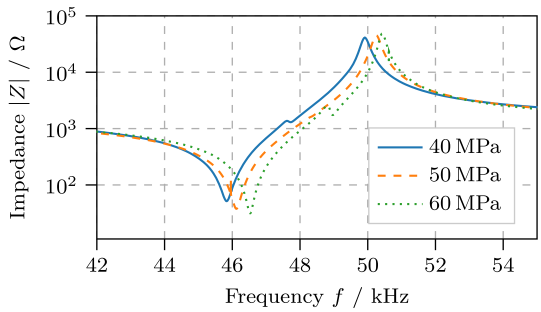


**Figure 4:** Electrical impedance spectra of the piezoceramic sample measured after 45 h of operation for different mechanical preloads of the transducer.

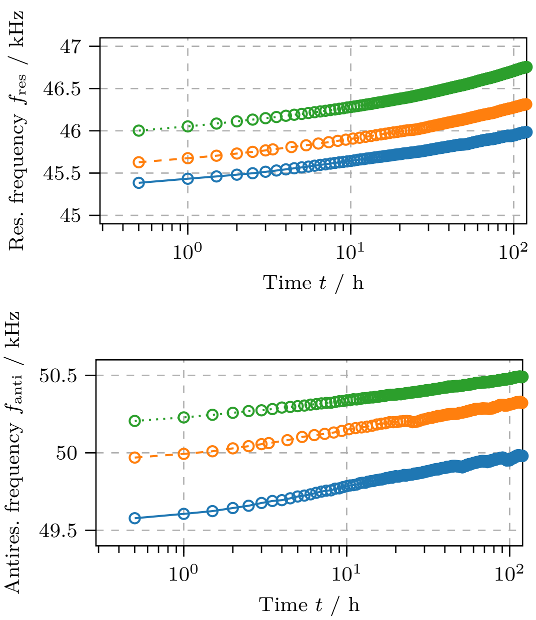


**Figure 5:** Time evolution of the resonance frequency $f_{\mathrm{res}}$ and the antiresonance frequency $f_{\mathrm{anti}}$ during the first 45 h of the long-term experiment for mechanical preloads of 40 MPa (—⊖—), 50 MPa (- ⊖ -), and 60 MPa (··⊙··).

# 4 Inverse parameter identification

The inverse identification procedure used to estimate piezoceramic material parameters from measured impedance response is detailed in the following section. Subsection 4.1 addresses the general inverse procedure, including the estimation of the initial parameter vector $\boldsymbol{p}_0$ and the formulation of the optimisation problem. The solution approach is presented in Subsection 4.2, with particular focus on the sensitivity-informed block coordinate descent method developed to address the challenges inherent to piezoelectric parameter identification.

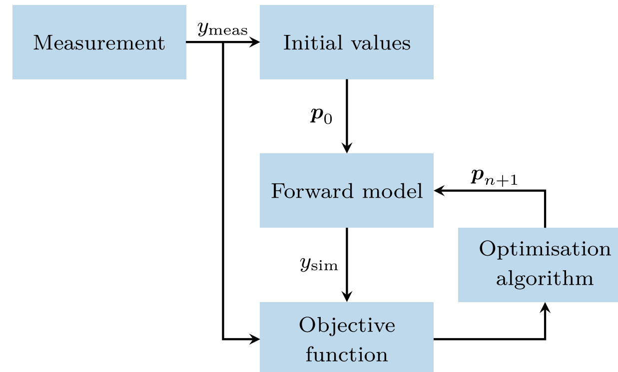


**Figure 6:** Schematic representation of the inverse procedure for estimating material parameters.

## 4.1 Inverse procedure

The determination of suitable material parameters cannot be achieved by direct measurement of specific coefficients. Therefore, an inverse identification approach, depicted in Figure 6, is used. Measuring characteristic quantities $y_{\mathrm{meas}}$ such as the electrical impedance spectrum $Z(f)$, allows the comparison to the numerically obtained forward model output $y_{\mathrm{sim}}$. The material parameters $\boldsymbol{p}$ are iteratively refined until a predefined termination criterion is satisfied and a sufficient agreement between simulation and measurement is achieved with regard to an objective function. The mathematical analysis of these inverse problems is an important prerequisite regarding reliability of results and can be found in [20], [21].

The first step in the process is the estimation of the initial values $\boldsymbol{p}_0$ from the measurements described in Section 3. The accuracy of the initial values has a direct impact on the efficiency of the subsequent algorithm for solving the non-convex inverse problem. Observations have shown that a higher accuracy in the initial values is correlated to time-efficiency in convergence. Thus, it is advantageous to estimate the initial values as close as possible to the target values. There are a number of approaches to achieve this objective.

Some analytical approximations can be found, which facilitate the formulation of relationships between the characteristic quantities of the impedance, such as resonance and antiresonance frequencies, and certain material parameters, analogous to the approach already employed in the standardised procedure for determining material parameters [22]. The estimation of parameters from these analytical expressions relies on a number of simplifications, including the assumption of an isotropic material. While this assumption is found to be valid for the initial estimate, it has also been demonstrated that post-optimising these initial values using an analytical forward model is indispensable to achieve high accuracy [18].

Another approach for initial parameter estimation is to train a neural network via a number of impedance responses, simulated using randomised material parameters [11]. Although the generation of training data and the initial training phase are computationally demanding, the advantages of this approach are notable in terms of the reuse of the network and the speed as well as the accuracy of the estimation process.

Using the initial parameter vector $\boldsymbol{p}_0$, the corresponding electrical impedance response is computed by means of the finite element forward model. Depending on the implementation environment, frequency, and mesh resolution used, the duration of this step is typically a matter of minutes. The model evaluates the coupled electromechanical field equations and yields the simulated response $y_{\text{sim}}(\boldsymbol{p})$, which is subsequently compared to the experimentally measured impedance response $y_{\text{meas}}$.

The parameter identification is formulated as a nonlinear least-squares problem. The objective is to determine a parameter vector $\boldsymbol{p}$ that minimises

$$J(\boldsymbol{p}) := \frac{1}{2}\left\|y_{\text{sim}}(\boldsymbol{p}) - y_{\text{meas}}\right\|^2_{\mathbb{R}^{|\mathcal{W}|}}, \tag{6}$$

i.e., the data discrepancy between simulation and measurement, where $\mathcal{W} \subset \mathbb{R}$ denotes the discrete and finite set of excitation frequencies, which is bounded and of finite cardinality. The Euclidean norm quantifies the deviation between simulated and measured impedance values across all frequency points.

The resulting optimisation problem is solved iteratively. In each iteration, $y_{\text{sim}}$ is evaluated on the updated parameter vector $\boldsymbol{p}$, and the parameters are adjusted according to the selected optimisation scheme. Powerful optimisation frameworks are *coordinate descent* (CD) [23] and *block coordinate descent* (BCD) methods [24]. The basic idea behind BCD methods is to obtain the solution to an optimisation problem by repeatedly solving a sub-problem with respect to a previously selected block of parameters. To solve inverse problems, the BCD method iteratively applies a regularised sub-optimisation procedure separately to each block, resulting in an update of the parameters within the respective block. This procedure is iteratively continued until a redefined convergence criterion is satisfied, which usually requires no more than 50 iterations. The CD method can be viewed as a special case of the BCD method as the blocks therein are trivial, i.e., only one element is contained in the blocks. These procedures enable the systematic identification of effective material properties under realistic mechanical preload and thermal operating conditions.

## 4.2 Solution approach to the inverse problem

Parameter identification problems in piezoelectricity suffer from considerably varying sensitivities of the forward model with respect to different parameters [25], [26]. The sensitivity of $y_{\text{sim}}$ measures the change in $y_{\text{sim}}$ when single parameters, i.e., single entries of $\boldsymbol{p}$, change. Thus, it can be modelled via first-order derivatives with respect to the material parameters, that is the partial sensitivity of $y_{\text{sim}}$ with respect to $\boldsymbol{p}_j$ at frequency $f$

$$s_{j,f} := \left|\frac{\partial y^f_{\text{sim}}(\boldsymbol{p})}{\partial \boldsymbol{p}_j}\right| \tag{7}$$

and the total sensitivity of $y_{\text{sim}}$ with respect to $\boldsymbol{p}_j$, as the sum of $s_{j,f}$ over the frequency domain. As this severe heterogeneity, apparent in Figure 7, drastically complicates the solution of the inverse problem, a cyclic *block coordinate descent* method is investigated to address this drawback [25]. For sub-optimisation, the *globalised regularised structure-exploiting Powell-Symmetric-Broyden* (GRSE-PSB) method represents a highly advantageous choice [27]. The latter is particularly suited for solving nonlinear inverse problems where second-order derivative information is beneficial, for instance due to nonlinearity of $y_{\text{sim}}$, inaccessibility of measurement or model noise, or an insufficient quality of the initial guess combined with high nonconvexity [27]. The motivation underlying this approach is to avoid the high computational cost of full Hessian evaluations required by classical Newton methods, to incorporate analytical Hessian structure – which classic

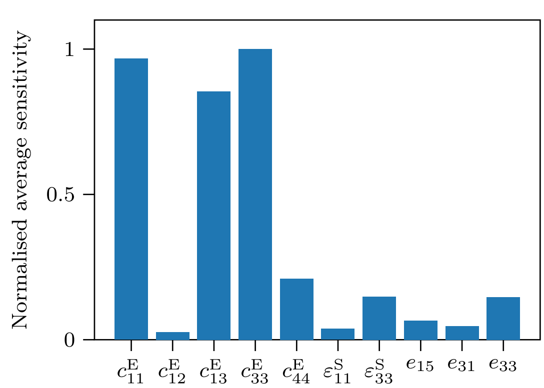


**Figure 7:** Normalised sensitivity of $y_{\text{sim}}$ averaged with respect to the frequency domain cardinality and normalised by its corresponding maximum.

Quasi-Newton methods typically ignore – and to circumvent the Levenberg-Marquardt approximation error in nonlinear real-world problems. To ensure robustness and proper regularisation, the regularisation parameter is algorithmically controlled such that it yields globalisation [27], [28]. Consequently, the resulting BCD-GRSE method is well-suited for multiphysics parameter identification problems.

A central question in this framework concerns the grouping of the parameters into blocks. To address this task fully algorithmically, a sensitivity-driven approach has been developed, considering both the influence of individual parameters and the interactions between them [25]. Accordingly, the cross-sensitivity of $y_{\mathrm{sim}}$ needs to be introduced to quantify the mutual influence of two specific parameters, which can be described by second-order derivatives with respect to the material parameters. High cross-sensitivity indicates strong coupling, i.e., a change in one parameter can substantially alter the impact of another, complicating the optimisation.

To guide block formation, it is proposed to form parameter blocks that internally exhibit small gradient roughness, while remaining externally as decoupled as possible [25]. The latter is achieved via minimising the total cross-sensitivity across two blocks. To quantify roughness in gradients, the intra-block roughness measure, an additional curvature-based measure, is developed [25]. It reflects how rapidly the gradient of the objective function changes within a block. Blocks with high roughness exhibit strong nonlinearity or potential numerical instability, while blocks with low roughness are desirable as the sub-optimisation problem will be better conditioned. This results in a combinatorial optimisation problem minimising interactions between blocks (min. cross-sensitivity), while ensuring that gradients remain stable (min. roughness). After the block partitioning process, updates may be prioritised based on the overall influence of each block, typically updating the most sensitive blocks first. While this sensitivity-informed BCD framework overcomes the drawback of large sensitivity differences, sensitivities themselves remain unchanged. As a result, uncertainties are handled much better by this approach. However, especially for parameters for which the forward operator exhibits low sensitivity, some uncertainty remains. For the application considered here, this holds for the identification of $\varepsilon_{11}$ and $e_{15}$ [18], [25], as reflected in the results presented in Section 5. Although the sensitivity with respect to $c_{12}$ is among the lowest, Figure 8 shows that its high-frequency region is dominated exclusively by $c_{12}$, thereby increasing its identifiability. Therefore, the identification of these parameters remains challenging

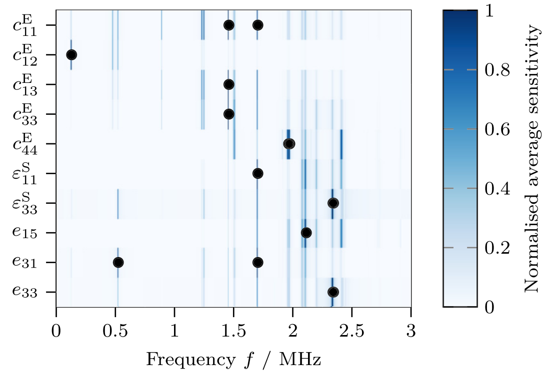


**Figure 8:** Partial sensitivities scaled by $\max_j s_{j,f}$ for each frequency $f$.

and motivates further, potentially statistical, uncertainty minimisation.

# 5 Results

The results of the inverse parameter identification applied to the experimental data acquired as described in Section 3 are presented in the following section. Subsection 5.1 addresses the temperature-dependent material parameters and their incorporation into a coupled thermo-electromechanical simulation framework (Subsection 5.2). The corresponding results for mechanical stress-dependent parameters, obtained from the Langevin-type transducer configuration, are discussed in Subsection 5.3.

## 5.1 Temperature-dependent linear material parameters

The impedance measurements acquired using the temperature-controlled setup of Subsection 3.1 are used to estimate the material parameters by means of the inverse procedure described in Section 4. The process is applied to each measurement separately, yielding data sets for each temperature step as listed in Table 4 in Appendix A. To quantify the temperature-dependent changes, the coefficients of linear polynomials

$$p_i(\vartheta) = p_{i,25\,^\circ\mathrm{C}} + p_i' \cdot (\vartheta - 25\,^\circ\mathrm{C}) \tag{8}$$

are calculated for each parameter $p_i$, where $\vartheta$ is the temperature. The resulting regression coefficients, together with a graphical indication of the respective trend, are summarised in Table 1. The observations indicate that temperature has only a limited influence on the overall material behaviour.

The mechanical coefficients $c_{11}^E$ to $c_{44}^E$ show only minor variations over the temperature range, as reflected by the

**Table 1:** Results of the linear regression of the temperature dependent material parameters for a piezoceramic ring of PIC181. For the full numerical results see Table 4.

| | $p_{i,25\,^\circ\mathrm{C}}$ | $p_i'/\mathrm{K}^{-1}$ | Unit | Regression |
|---|---|---|---|---|
| $c_{11}^E$ | 142.49 | $2.44 \cdot 10^{-3}$ | GPa | |
| $c_{12}^E$ | 82.62 | $5.39 \cdot 10^{-3}$ | GPa | |
| $c_{13}^E$ | 81.05 | $-6.85 \cdot 10^{-3}$ | GPa | |
| $c_{33}^E$ | 138.79 | $5.29 \cdot 10^{-3}$ | GPa | |
| $c_{44}^E$ | 30.17 | $8.40 \cdot 10^{-3}$ | GPa | |
| $\varepsilon_{11}^S$ | 12.91 | $38.67 \cdot 10^{-3}$ | nF m$^{-1}$ | |
| $\varepsilon_{33}^S$ | 5.10 | $17.29 \cdot 10^{-3}$ | nF m$^{-1}$ | |
| $e_{15}$ | 13.02 | $16.70 \cdot 10^{-3}$ | C m$^{-2}$ | |
| $e_{31}$ | −5.27 | $-0.14 \cdot 10^{-3}$ | C m$^{-2}$ | |
| $e_{33}$ | 13.43 | $23.26 \cdot 10^{-3}$ | C m$^{-2}$ | |
| $\alpha_K$ | 129.33 | $-194.82 \cdot 10^{-3}$ | ps | |

small regression coefficients and the flat trend indicators in Table 1. This trend is consistent with the temperature-dependent characteristics provided by the manufacturer, which indicate for example a shift of the resonance frequency towards higher values with increasing temperature, in agreement with the slightly increasing stiffness parameters identified in the present work [29]. More pronounced changes are observed in the dielectric properties, particularly in $\varepsilon_{33}^S$, which increases monotonically with temperature. In contrast, the results for $\varepsilon_{11}^S$ demonstrate irregular variations. These fluctuations can be attributed to the low sensitivity of the electrical impedance to this parameter [25] and the increased uncertainty in its identification [11]. Comparable behaviour is evident for the piezoelectric coefficients $e_{31}$ and $e_{15}$, which can be attributed to analogous sensitivity-related restrictions. A clear and monotonic increase is observed in $e_{33}$, which can be considered significant given the influence of this coefficient on the electromechanical behaviour of the sample. The damping parameter $\alpha_K$ decreases with increasing temperature, as indicated by its negative regression coefficient.

## 5.2 Thermo-piezoelectric field simulations

The temperature-dependent material parameters identified above enable a coupled simulation in which the electromechanical and thermal fields are solved simultaneously. Since the material parameters vary with temperature, they cannot be assumed constant during the simulation but must be evaluated at each time step based on the solution of Equation (8). Then, the thermo-electromechanical coupling is applied by the mechanical loss term. A numerical method to simulate coupled electrical, mechanical and thermal fields while consistently accounting for temperature-dependent material parameters is implemented using FEniCS [30], [31]. The same simulation framework is used for the present work.

The coupled thermo-electromechanical simulation employs a time step in the order of 10 ns. During excitation, the piezoceramic disc undergoes a transient phase before reaching a stationary oscillation state. In contrast to the electromechanical dynamics, the thermal behaviour evolves on a much slower time scale, typically in the range from 100 µs to 1 ms. Hence, resolving application-relevant operating times at the electromechanical time step would require an impractical number of time steps and result in excessive computational cost. To manage this computational demand, a multi-scale time-stepping strategy is adopted [32].

Since the time-averaged power loss density becomes constant when the stationary oscillation state is reached, it can be used in a separate thermal simulation in which a larger time step, e.g., 1 ms can be applied. This reduces the simulation time significantly. The coupled simulation is initiated at ambient temperature with an electromechanical simulation with the fine time step until a stationary oscillation state is reached, identified by monitoring the heat source term of the thermal simulation. The values for the specific heat capacity $c_P$ and the thermal conductivity $\lambda_{\mathrm{th}}$ are taken from the manufacturer's specifications [29]. It is acknowledged that these quantities are subject to uncertainty; the experimental determination of these thermal material properties is identified as a subject for future work. Once stationarity is detected, the simulation is continued with a purely thermal analysis driven by the time-averaged constant power loss density. This thermal simulation with a time step of 1 ms proceeds until the temperature at any node in the mesh increases by 1 K – a threshold motivated by the experimentally observed parameter variations summarised in Table 1. The coupled simulation is then resumed with the updated material parameters based on the temperature distribution, and the procedure is repeated iteratively.

For an application-oriented example, a piezoceramic ring (PIC181, PI Ceramic, Germany) with an outer radius of 6.35 mm, an inner radius of 2.6 mm, and a thickness of 1 mm is excited at its first thickness resonance (2.23 MHz) with an applied voltage amplitude of 20 V. The resulting temperature distribution, recorded after 40 s, is shown in Figure 9. Due to the rotational symmetry of the sample, the simulation is performed on a two-dimensional axisymmetric cross-section, with the axis of symmetry located at the left boundary of the domain ($r = 0$). It can be observed that the piezoceramic ring experiences a substantial overall increase in temperature. Furthermore, the temperature distribution is non-uniform: the inner region of the ring exhibits higher

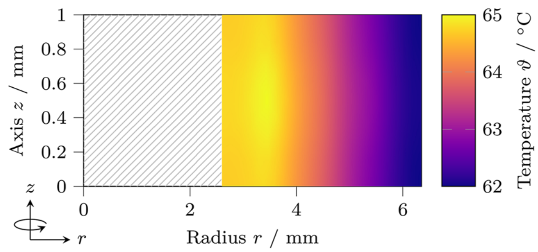


**Figure 9:** Simulation result for the thermal field of the cross-sectional area of a piezoelectric ring following harmonic excitation with an amplitude of 20 V and a frequency of 2.23 MHz after 40 s.

temperature than the outer region, which can be attributed to the smaller radius and the associated concentration of dissipated energy. This behaviour highlights the importance of accounting for geometrical effects when evaluating the thermal response of piezoceramic components under high-frequency excitation.

## 5.3 Mechanical stress-dependent linear material parameters

The application of the parameter identification strategy outlined in Section 4 to a Langevin-type transducer (Figure 3) introduces additional complexity compared to the characterisation of unconstrained piezoceramic specimens. The multi-component structure results in an impedance response dominated by a single thickness resonance within the operationally relevant frequency range, as shown in Figure 4. Radial and torsional modes are largely suppressed in this configuration, which restricts the number of identifiable piezoceramic material parameters. To address this limitation, a sensitivity analysis is employed to identify the parameters with the greatest influence on the observable resonance. It was found that the parameters in the longitudinal 33-direction, namely $c_{33}^S$, $e_{33}$ and $\varepsilon_{33}^S$, exhibit the highest sensitivity, making their estimation feasible within the limited frequency range.

The estimation is carried out in two sequential steps. An initial simulation is performed using the material parameters identified for an unconstrained PIC184 piezoceramic specimen and steel material parameters obtained from data sheets [33]. As shown in Figure 10, this initial simulation (——) shows a notable deviation from the measurement data (– – –), which can be attributed to the pre-stress of 40 MPa required to ensure full mechanical contact between transducer components. Therefore, the steel parameters are identified first, estimated in order of decreasing sensitivity, with the transversal velocity $c_T$ prioritised, followed by the

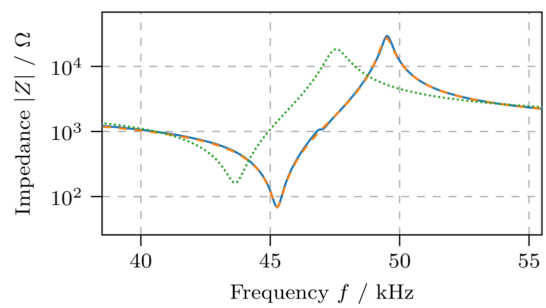


**Figure 10:** Comparison of measured (.........) and simulated impedance data of a Langevin-type transducer for a static stress of 40 MPa using the determined (.........) and initial (——) material parameters.

**Table 2:** Determined material parameters for steel.

| Parameter | Value | Parameter | Value |
|---|---|---|---|
| $c_L$ | 6,123.79 m s$^{-1}$ | $\alpha_M$ | $3.99 \cdot 10^{-8}$s$^{-1}$ |
| $c_T$ | 3,473.65 m s$^{-1}$ | $\alpha_K$ | 5.46 ps |

**Table 3:** Determined stress-dependent piezoceramic material parameters in 33-direction for PIC184.

| Parameter | Mechanical stress | | |
|---|---|---|---|
| | 40 MPa | 50 MPa | 60 MPa |
| $c_{33}^E$/GPa | 126.29 | 128.37 | 131.73 |
| $e_{33}$/C m$^{-1}$ | 16.23 | 17.77 | 18.31 |
| $\varepsilon_{33}^E$/nF m$^{-1}$ | 6.9 | 7.18 | 7.3 |

longitudinal velocity $c_L$ and the damping parameters. The resulting parameters for steel are listed in Table 2.

Subsequently, the piezoceramic parameters in the 33-direction are estimated simultaneously using impedance measurements taken at mechanical stress levels of 40 MPa, 50 MPa, and 60 MPa (see Subsection 3.2). The estimated piezoelectric material parameters are listed in Table 3. The simulated impedance response obtained using the optimised steel and piezoelectric parameters is also shown in Figure 10 (– – –), demonstrating the improvement over the initial simulation.

The identified parameters increase monotonically with rising mechanical load across all three stress levels, consistent with the stress-dependent nonlinear behaviour of the material. The application of the estimated parameters in the simulation and the comparison with the measurement data reveal a high degree of agreement across all stress conditions, thus validating the proposed identification approach. These findings provide an impression of the nonlinearities present under mechanical stress and establish the basis for nonlinear material modelling.

# 6 Towards nonlinear behaviour

Up to this point, extensive studies have been made to estimate linear electrical, mechanical and piezoelectrical material parameters under various operational conditions, such as different temperatures or mechanical stress levels. While this linear characterisation provides an initial approximation of the nonlinear material response, a dedicated nonlinear model is required to capture and recreate observed nonlinear effects. The present section addresses this need by reviewing relevant modelling approaches from the literature and introducing a cubic nonlinear material model suitable for high-power ultrasonic transducers.

The nonlinear effects observed in piezoceramic components under such conditions include the generation of superharmonics, the tilting of resonance curves, as well as associated jump phenomena and bifurcations in the frequency response. The tilting resonance curves are of particular significance, which indicate a memory effect of the dynamical system: the system response depends not only on the current excitation state but also on its history. Previous studies by Simkovics et al. [34] and Kaltenbacher et al. [35] investigated nonlinear piezoceramic behaviour by modelling hysteresis loops of the electrical polarisation and the butterfly curve of the mechanical strain, and by making material parameters directly dependent on the electric field and mechanical stress. However, such nonlinearities become particularly apparent at strong electric fields, also referred to as large signal analysis, in which geometric nonlinearities must also be considered. These assumptions exceed the requirements of the present work, where the piezoceramic elements are excited at high frequencies with comparatively weak electric fields.

A similar approach for the present problem is discussed by Von Wagner et al. [36] and Samal et al. [37], who analysed nonlinear piezoceramic behaviour for weak electric fields at higher frequencies. They observe that the nonlinear behaviour is similar to that of a Duffing oscillator, leading them to formulate constitutive equations based on a quadratic- and cubic-order term in the elastic formulation. Using their approach they are able to reproduce the nonlinear behaviour but had to rely on linearisation approaches in order to derive a suitable finite element formulation. Additionally, the estimation of nonlinear parameters and the nonlinear tensor filling remain unclear, which makes this approach unsuitable for further analysis and parameter estimation using an inverse procedure. In [15], [38] it is shown that third-order elastic constants [39] can be used to model nonlinear behaviour in piezoceramic materials and that a finite element formulation can be derived. Although the simulation and measurement results were not optimal, the same approach can be used to derive a finite element formulation for fourth-order elastic constants, for which the nonlinear system is expected to exhibit Duffing-like behaviour in order to improve the results. This approach enables the estimation of nonlinear parameters and does not rely on linearisation methods to derive a suitable finite element method formulation.

## 6.1 Modelling nonlinear effects

As mentioned above, prominent nonlinear effects are the jump phenomena occurring due to a tilting of resonance curves. Those jumps are the reaction of the system when operating in unstable regions. From such tilting, shown exemplarily in Figure 11 using the differential equation of the Duffing oscillator, it can be seen that the frequency-dependent amplitude of system $A(\omega)$ can have up to three different solutions for one specific frequency. It is observed that the path taken depends on the direction of the frequency sweep, reflecting the memory effect of the system. The backbone curve shows the change of the natural frequency of the system depending on the amplitude. When a softening nonlinear spring is assumed (which is the case in Figure 11), the behaviour of the Duffing oscillator is similar to the impedance of piezoelectric systems [40].

Based on these considerations, a cubic nonlinear material model is adopted, extending the linear constitutive Equation (1a) with an additional term written in Einstein notation:

$$T_i = -\underline{e}^{\mathsf{T}}_{ij} E_j + \underline{c}^{E}_{ij} S_j + \alpha_K \underline{c}^{E}_{ij} \partial_t S_j + \underline{\widetilde{c}}_{ijkl} S_j S_k S_l, \tag{9}$$

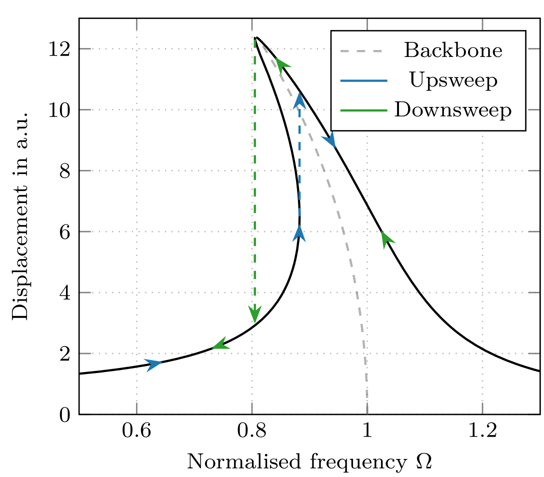


**Figure 11:** Tilting resonance curve of a duffing oscillator with path dependent trajectories for up- and downsweeps.

where $\tilde{c}$ is a fourth-order tensor including the fourth-order elastic constants (FOEC).

The estimation of the FOEC via an inverse method requires a suitable numerical forward model. For linear simulations, frequency-domain finite element methods are well established, however, the nonlinear case presents additional challenges. The system's nonlinearity renders classical frequency-domain computations impossible, necessitating either multiple time-domain simulation runs at various frequencies until steady state is reached or methods such as the *harmonic balancing method* [41], in which a truncated Fourier series is used as an ansatz for the system response. Furthermore, the instability of the system in the overhanging region requires path-following methods to solve the nonlinear system in such regions [42]. These challenges will be addressed in future work by implementing a numerical framework combining the harmonic balancing method with the finite element method and a path-following algorithm. In addition to the full fourth-order elastic constant tensor, reduced-order models will be investigated to minimise the number of independent parameters, thereby reducing simulation cost and simplifying the inverse parameter estimation.

# 7 Conclusions

The present work demonstrates that inverse measurement procedures, combining impedance-based experimental techniques with sensitivity-informed optimisation strategies, constitute a powerful and flexible approach for the characterisation of piezoceramic materials under realistic operating conditions. The determination of effective linear material parameters as a function of temperature and mechanical and electrical pre-stress enables possible approximations to describe and model the non-linear behaviour of such components in real-world operation.

Furthermore, it has been demonstrated that the identified parameter sets can be applied directly in coupled thermo-electromechanical simulations, thereby enabling the prediction of temperature profiles and their effects on material behaviour during high-power ultrasonic operation. The good agreement between the measured and simulated impedance spectra, using the identified material parameters, under all operating conditions investigated, validates the proposed identification approach.

As a first step towards the development of a nonlinear material model, a cubic nonlinear constitutive model based on fourth-order elastic constants is introduced. This model is motivated by the observed Duffing-oscillator-like behaviour of piezoceramic components under elevated signal and high frequency excitation. The development of a corresponding finite element forward model, combining the harmonic balance method with path-following algorithms, is identified as the next step towards a simulation-based design framework for high-power ultrasonic systems and remains the subject of ongoing work within the Research Unit. In addition, experimental setups are planned to measure the jump phenomena observed in the nonlinear operating regime, with the aim of providing a robust experimental basis for the validation of the nonlinear material models under development.

**Acknowledgments:** The authors would like to thank Prof. Michael Winkler, Torben Fricke and Felix Meyer (AG Partielle Differentialgleichungen, Paderborn University) for valuable scientific discussions on the analysis of the underlying partial differential equations, as well as Lars Meihost (Measurement Engineering Group, Paderborn University) for his technical support in the development and implementation of the experimental setups.
**Research ethics:** Not applicable.
**Informed consent:** Not applicable.
**Author contributions:** All authors have accepted responsibility for the entire content of this manuscript and approved its submission.
**Use of Large Language Models, AI and Machine Learning Tools:** DeepL, claude.ai to improve language.
**Conflict of interest:** The authors state no conflict of interest.
**Research funding:** Deutsche Forschungsgemeinschaft (DFG, German Research Foundation) – 444955436 (FOR 5208: NEPTUN) .
**Data availability:** The raw data can be obtained on request from the corresponding author.

# A Estimated material parameters

This appendix provides the complete set of temperature-dependent material parameters identified for the piezoceramic ring specimen (PIC181), as referenced in Subsection 5.1. The parameters in Table 4 are obtained by applying the inverse identification procedure of Section 4 independently to each temperature step, covering the range from 25 °C to 85 °C in increments of 5 K. The corresponding regression coefficients and trend indicators derived from these data are summarised in Table 1.

**Table 4:** Results for the estimated temperature-dependent material parameters for piezoceramic ring of material PIC181 with a thickness $t$ of 1 mm, an outer radius $r_o$ of 6.35 mm, and an inner radius $r_i$ of 2.6 mm.

| | 25 °C | 30 °C | 35 °C | 40 °C | 45 °C | 50 °C | 55 °C | 60 °C | 65 °C | 70 °C | 75 °C | 80 °C | 85 °C | Unit |
|---|---|---|---|---|---|---|---|---|---|---|---|---|---|---|
| $c_{11}^E$ | 142.8 | 142.9 | 142.7 | 142.2 | 142.4 | 142.1 | 142.3 | 142.2 | 142.6 | 142.8 | 142.4 | 142.9 | 142.9 | GPa |
| $c_{12}^E$ | 83.3 | 81.9 | 84.9 | 82.6 | 83.0 | 80.9 | 81.2 | 81.1 | 83.1 | 84.8 | 82.9 | 83.1 | 83.3 | GPa |
| $c_{13}^E$ | 81.2 | 81.2 | 81.0 | 80.8 | 80.9 | 80.6 | 80.7 | 80.7 | 80.8 | 80.7 | 80.7 | 80.7 | 80.8 | GPa |
| $c_{33}^E$ | 138.8 | 138.8 | 138.8 | 138.9 | 139.0 | 138.8 | 138.9 | 139.0 | 139.0 | 138.9 | 139.1 | 139.0 | 139.2 | GPa |
| $c_{44}^E$ | 30.2 | 30.2 | 30.2 | 30.3 | 30.3 | 30.4 | 30.4 | 30.5 | 30.5 | 30.5 | 30.6 | 30.5 | 30.7 | GPa |
| $\varepsilon_{11}^S$ | 13.4 | 13.2 | 12.8 | 13.4 | 14.5 | 12.9 | 13.9 | 14.2 | 14.8 | 13.8 | 15.5 | 14.4 | 16.0 | nF m$^{-1}$ |
| $\varepsilon_{33}^S$ | 5.1 | 5.2 | 5.3 | 5.4 | 5.4 | 5.5 | 5.6 | 5.7 | 5.8 | 5.9 | 6.0 | 6.1 | 6.2 | nF m$^{-1}$ |
| $e_{15}$ | 13.2 | 13.1 | 13.0 | 13.2 | 13.6 | 13.1 | 13.5 | 13.6 | 13.8 | 13.5 | 14.0 | 13.7 | 14.2 | C m$^{-2}$ |
| $e_{31}$ | −5.3 | −5.2 | −5.1 | −5.3 | −5.5 | −5.1 | −5.3 | −5.3 | −5.3 | −5.0 | −5.4 | −5.1 | −5.4 | C m$^{-2}$ |
| $e_{33}$ | 13.4 | 13.6 | 13.7 | 13.8 | 13.9 | 14.0 | 14.1 | 14.2 | 14.3 | 14.5 | 14.6 | 14.7 | 14.8 | C m$^{-2}$ |
| $\alpha_K$ | 125.9 | 126.1 | 130.1 | 128.0 | 126.8 | 126.6 | 123.9 | 122.5 | 118.6 | 122.0 | 120.0 | 119.7 | 114.9 | ps |

# References


[1] S. Johann Rupitsch, *Piezoelectric Sensors and Actuators*, *Topics in Mining, Metallurgy and Materials Engineering*, 1st ed., Berlin, Germany, Springer, 2018.

[2] M. Kaltenbacher, *Numerical Simulation of Mechatronic Sensors and Actuators*, Heidelberg, Springer Berlin, 2007.

[3] L. Reinhard, “Simulation of piezoelectric devices by two- and three-dimensional finite elements,” *IEEE Trans. Ultrason. Ferroelectr. Freq. Control*, vol. 37, no. 3, pp. 233–247, 1990.

[4] Q.-M. Wang, T. Zhang, Q. Chen, and X. H. Du, “Effect of DC bias field on the complex materials coefficients of piezoelectric resonators,” *Sens. Actuators, A*, vol. 109, nos. 1–2, pp. 149–155, 2003.

[5] R. Simkovics, “Nichtlineares piezoelektrisches Finite-Elemente-Verfahren zur Modellierung piezokeramischer Aktoren,” PhD thesis, Düsseldorf, VDI-Verlag, 2002.

[6] C. Scheidemann, P. Bornmann, W. Littmann, and T. Hemsel, “Lead-free ceramics in prestressed ultrasonic transducers,” *Actuators*, vol. 14, no. 255, 2025, Art. no. 55.

[7] S. Hong Choy and H. L. W. Chan, “Nonlinear behavior of BNT-based lead-free piezoceramics under various ac fields,” *Curr. Appl. Phys.*, vol. 11, no. 3, pp. 869–877, 2011.

[8] W. Voigt, *Lehrbuch der Kristallphysik (mit Ausschluss der Kristalloptik)*, vol. 34, Leipzig, Berlin, B.G. Teubner, 1910.

[9] T. William, “IV. On the elasticity and viscosity of metals,” *Proc. R. Soc. London*, vol. 12, no. 14, pp. 289–297, 1865.

[10] W. Voigt, “Ueber die innere Reibung der festen Körper, insbesondere der Krystalle,” *Abh. Königlichen Ges. Wiss. Göttingen*, vol. 36, no. 1, pp. 3–47, 1889.

[11] L. Claes, K. Koch, O. Friesen, and L. Meihost, “Machine learning-supported inverse measurement procedure for broadband, temperature dependent piezoelectric material parameters,” *Acta Acust.*, vol. 9, 2025, Art. no. 65.

[12] S. Schoder and K. Roppert, “openCFS: Open source finite element software for coupled field simulation — Part acoustics,” arXiv: 2207 . 04443 [math.NA], 2022.

[13] C. Spieker *et al*., “Modeling and simulation of the behavior of piezoceramics with the discontinuous Galerkin method,” in *Lectures*, Wunstorf, AMA Service GmbH, 2025, pp. 126–129.

[14] B. A. Boley and J. H. Weiner, *Theory of Thermal Stresses. Dover Civil and Mechanical Engineering*, New York, Dover Publications, 2012.

[15] L. Claes, J. Lankeit, and M. Winkler, “A model for heat generation by acoustic waves in piezoelectric materials: Global large-data solutions,” *Math. Models Methods Appl. Sci.*, vol. 35, no. 11, pp. 2465–2512, 2025.

[16] O. Friesen, *et al*., “Estimation of piezoelectric material parameters under varying electric field conditions,” in *DAS/DAGA 2025 - 51st Annual Meeting on Acoustics*, Kopenhagen, Deutsche Gesellschaft für Akustik e.V, 2025, pp. 994–997.

[17] O. Friesen, L. Claes, C. Scheidemann, N. Feldmann, T. Hemsel, and B. Henning, “Estimation of temperature-dependent piezoelectric material parameters using ring-shaped specimens,” in *2023 International Congress on Ultrasonics (ICU)*, vol. 2822, Beijing, IOP Publishing, 2024.

[18] O. Friesen, L. Claes, N. Feldmann, and B. Henning, “Estimation of piezoelectric material parameters of ring-shaped specimens,” *tm - Tech. Messen*, vol. 92, no. 6, pp. 203–213, 2025.

[19] C. Scheidemann *et al*., “Investigation of the setting behaviour of mechanically biased piezoelectric ultrasonic transducers,” in *2025 International Congress on Ultrasonics (ICU)*, Paderborn, AMA Service GmbH, 2025.

[20] R. Kuess, D. Walter, and A. Walther, “Modelling and analysis of an inverse parameter identification problem in piezoelectricity,” Optimization Online, https://optimization-online.org/?p=33654, 2026.

[21] T. J. Fricke, R. Kuess, and F. Meyer, “Existence of large data solutions to a thermo-piezoelectric problem and its application to inverse problems,” arXiv: 2602.14848, 2026.

[22] IEEE Standard on Piezoelectricity. Norm. 1988.

[23] S. J. Wright, “Coordinate descent algorithms,” *Math. Program.*, vol. 151, no. 1, pp. 3–34, 2015.

[24] J. Nutini, I. Laradji, and M. Schmidt, “Let’s make block coordinate descent converge faster: Faster greedy rules, message-passing,

active-set complexity, and superlinear convergence," *J. Mach. Learn. Res.*, vol. 23, no. 1, 2022, Art. no. 131.
[25] R. Kuess *et al*., "Sensitivity-informed identification of temperature-dependent piezoelectric material parameters," Optimization Online, 2026, https://optimization-online.org/?p=33478.
[26] R. Kuess *et al*., "Identification of temperature-dependent material parameter functions in piezoelectricity," in *2025 International Congress on Ultrasonics (ICU)*, Paderborn, AMA Service GmbH, 2025, pp. 134–137.
[27] R. Kuess and A. Walther, "On regularized structure exploiting quasi-Newton methods for inverse problems," Optimization Online, 2025, https://optimization-online.org/?p=29842.
[28] C. Kanzow and D. Steck, "Regularization of limited memory quasi-Newton methods for large-scale nonconvex minimization," *Math. Program. Comput.*, vol. 15, no. 3, pp. 417–444, 2023.
[29] PI Ceramic, "Piezokeramische Materialien und Bauelemente," in *Grundlagen, Eigenschaften und Anwendungen*, Lederhose, PI GmbH & Co. KG, 2011.
[30] C. Spieker *et al*., "Modellierung und Simulation des temperaturabhängigen Materialverhaltens von Piezokeramiken mit FEniCS," in *Fortschritte der Akustik – DAGA*, Dresden, Deutsche Gesellschaft für Akustik e.V, 2026.
[31] M. Alnæs *et al*., "The FEniCS project version 1.5," *Arch. Numer. Software*, vol. 3, no. 100, pp. 9–23, 2015.
[32] J. Hölscher *et al*., "Multiscale thermo-piezoelectric simulations using the finite element method," in *Lectures*, Paderborn, AMA Service GmbH, 2025, pp. 130–133.
[33] G. Lucefin, "Lucefin steel," Technical card, revision, 2013.
[34] R. Simkovics *et al*., "Nonlinear finite element analysis of piezoelectric transducers," in *1999 IEEE Ultrasonics Symposium. Proceedings. International Symposium (Cat. No.99CH37027)*, vol. 2, New York, IEEE, 1999, pp. 1057–1060.
[35] B. Kaltenbacher *et al*., "Identification of material nonlinearities in piezoelectric ceramics," in *IEEE Symposium on Ultrasonics, 2003*, vol. 1, Honolulu, HI, USA, IEEE, 2003.
[36] U. von Wagner and P. Hagedorn, "Piezo-Beam systems subjected to weak electric field: Experiments and modelling of non-linearities," *J. Sound Vib.*, vol. 256, no. 5, pp. 861–872, 2002.
[37] M. K. Samal *et al*., "A finite element model for nonlinear behaviour of piezoceramics under weak electric fields," *Finite Elem. Anal. Des.*, vol. 41, no. 15, pp. 1464–1480, 2005.
[38] J. Hölscher *et al*., "Modeling nonlinear acoustic wave propagation with third-order elastic constants using the finite element method," in *96th Annual Meeting of the International Association of Applied Mathematics and Mechanics*, Stuttgart, GAMM, 2026.
[39] Y. Zhang, J. Jin, and H. Hu, "Third-order elastic, piezoelectric, and dielectric constants," *Appl. Math. Mech.*, vol. 40, no. 12, pp. 1831–1846, 2019.
[40] O. Friesen *et al*., "Experimental and Numerical investigation of jump phenomena in the frequency response of piezoelectric systems," in *96th Annual Meeting of the International Association of Applied Mathematics and Mechanics*, Stuttgart, GAMM, 2026.
[41] M. Krack and J. Gross, *Harmonic Balance for Nonlinear Vibration Problems*, Nature Switzerland AG, Springer, 2019.
[42] P. Wriggers, *Nonlinear Finite Element Methods*, Berlin, Heidelberg, Springer, 2010.

# Bionotes

**Olga Friesen**
Measurement Engineering Group, Paderborn University, Paderborn, Germany
**friesen@emt.uni-paderborn.de**
**https://orcid.org/0009-0007-5598-9484**

Olga Friesen is a research associate in the Measurement Engineering Group. After graduating in Electrical Engineering in 2022, she is now working on the quantitative characterisation of piezoelectric ceramics and the nonlinear properties of these materials.

**Jonas Hölscher**
Measurement Engineering Group, Paderborn University, Paderborn, Germany

Jonas Hölscher is a research associate in the Measurement Engineering Group. Following the completion of his master's degree in Electrical Engineering in 2025, he joined the Measurement Engineering Group to work on numerical simulations of nonlinear coupled piezoelectric systems.

**Claus Scheidemann**
Chair of Dynamics and Mechatronics, Paderborn University, Paderborn, Germany

Claus Scheidemann is a research assistant in the Dynamic and Mechatronics Group. After graduating in Mechanical Engineering in 2019, he works on the quantitative characterisation of piezoelectric ceramics to improve the simulation-based design of ultrasonic transducers.

**Raphael Kuess**
Mathematical Optimization,
Humboldt-Universität zu Berlin, Berlin,
Germany

Raphael Kuess is a research associate in the Mathematical Optimization Group at the Humboldt Universität zu Berlin. After graduating in Mathematics and in the Teacher’s Program for Mathematics and History in 2022, he is now working on temperature-dependent inverse problems in piezoelectricity, especially on the analysis, regularization, and structure-exploiting optimization.

**Carsten Spieker**
Theoretical Electrical Engineering Group,
Paderborn University, Paderborn, Germany

Carsten Spieker is a research associate in the Theoretical Electrical Engineering Group. After graduating in Electrical Engineering in 2023, he is now working on the development of piezoceramic simulations and the thermal properties of these materials.